Sensor and Simulation Notes

Note 390

December 1995

# Design Principles of Half Impulse Radiating Antennas

Everett G. Farr
Farr Research

Gary D. Sower
EG&G MSI

## Abstract

A candidate design for radiating single-ended, high-voltage, fast transient signals is to use a Half Impulse Radiating Antenna. This design avoids the mismatch that sometimes occurs in designs that require a balun or geometry conversion. We consider here the design principles involved in this antenna, including the $F/D$ ratio, and whether or not to offset the paraboloidal feed. In addition, we consider dielectric breakdown, and we calculate the field at the point most likely to induce dielectric breakdown. Finally, the radiated far fields are calculated both on- and off-boresight.

## I. Introduction

Recently developed pulsers have the capability to generate approximately 100 GW of peak power with an impulse width of about 150 ps Full Width Half Max, and with a repetition rate of about 1 kHz. However, all these hydrogen-gap pulsers produce output into a coaxial waveguide, which is a single-ended configuration. This configuration is difficult to match to an antenna, since most free-space antenna designs require a balanced feed. One can convert the signal to a balanced configuration with a coaxial unzipper [1] or point geometry converter, but there may be losses associated with these transitions. An alternative is to feed the signal into half a reflector Impulse Radiating Antenna, as first suggested in [2]. In this note we develop the design principles of half reflector Impulse Radiating Antennas, and we calculate the radiated far field.

We begin this note with general design considerations, including $F/D$ ratios, and offset designs. We also calculate the peak field where the conductor emerges from the oil. This is likely to be the point most sensitive to dielectric breakdown. We then calculate the radiated field both on- and off-boresight. Perhaps the most complex portion of the design deals with the feed-point lens. This material has already appeared as [3].

We begin now with the general design principles.

## II. General Design

We consider here a strategy for radiating a high-power single-ended transient source using a Half-Impulse Radiating Antenna (Half IRA). An example of a source we might wish to radiate with such an antenna is the HASP or H4 pulser currently being developed by Phillips Lab. The output of the H4 is a pulse with about 100 GW of peak power into a coaxial line. The pulse width is approximately 150 ps Full Width Half Max, and the source has a repetition rate of about 1 kHz.

A sketch of the proposed antenna is shown in Figure 2.1. For simplicity, we have assumed an $F/D$ of 0.25. The feed impedance of the two arms combined is 100 ohms in air. Note that these arms are the same angular width ($\pm 4^{o}$ from the cone center) as would be normally used in standard full IRA configurations, in which a single pair of arms with a full reflector has an impedance of 400 Ω. The lens is designed using the principles contained in [3]. An oil cap may or may not be used be used, depending upon dielectric breakdown considerations near the feed point. Configurations both with and without the oil cap are shown in Figure 2.2.

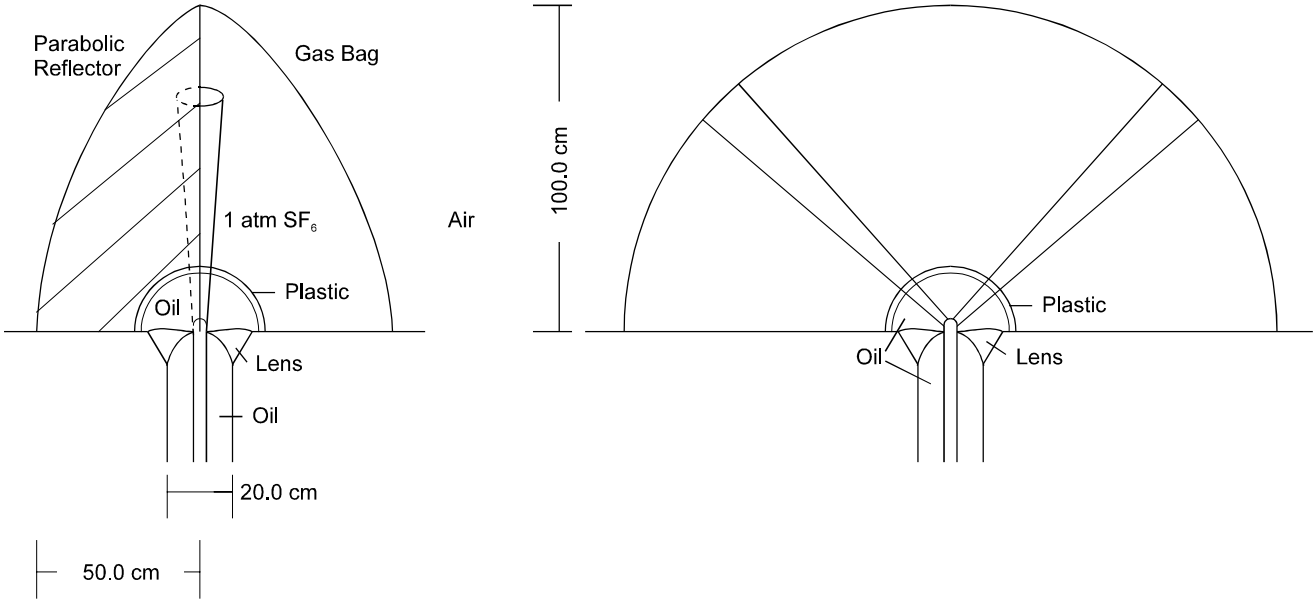


Figure 2.1 A sketch of the Half IRA, shown here with an oil cap.

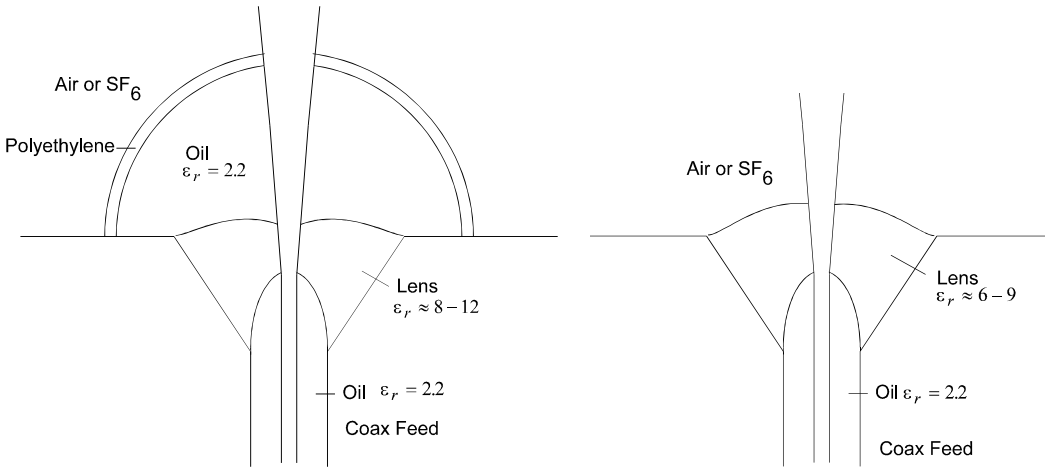


Figure 2.2. Two lens designs, with an oil cap (left) and without an oil cap (right).

To begin the design, we must first calculate the size of the coaxial feed necessary to propagate the signal without dielectric breakdown. There remains some controversy concerning the mechanisms of dielectric breakdown with very fast pulses, so there remains some uncertainty in this calculation.

On can reasonably consider two models of predicting dielectric breakdown. The first model assumes that any time the electric field is larger than some value, breakdown occurs. The maximum field level is a function of the material through which the electric field is propagating, as well as the length of the pulse. This first model may have to be modified by a second model. The second model suggests that if the time it takes for a light ray to cross the gap is shorter than the pulse duration, there is insufficient time for breakdown to occur. This modification may be important for pulses of very short duration.

As an example related to the H4 pulser, we might wish to maintain 100 GW through a feed impedance of 100 Ω in air, which is 67 Ω in oil, before going through the oil/air interface. (This assumes the conductors are continuous as they penetrate the interface.) We find the peak voltage using

$$V_{\max} = \sqrt{Z_c P_{\max}} \tag{2.1}$$

and we find a maximum voltage of 2.6 MV. To find the outer radius, we use [1, Eqn. 4.5]

$$\begin{aligned} E_{\max} &= E_{norm} \frac{V}{b} \\ E_{norm} &= \frac{e^{2\pi f_g \sqrt{\varepsilon_r}}}{2\pi f_g \sqrt{\varepsilon_r}} \end{aligned} \tag{2.2}$$

where $f_g = Z_c/(376.727\ \Omega)$, so $E_{norm}$ is found to 3.2 at 67 Ω. (One could also obtain the value of $E_{norm}$ from [1, Figure 4.2] ). If we assume a maximum electric field in oil of $E_{max}$ = 1 MV/cm, we then find an outer radius of 8.3 cm. (Note that there are some very recent experimental results suggesting that this is a very conservative number, perhaps by as much as a factor of ten. Ultimately, we will require further experimental data.)

Finally, the radius of the center conductor is calculated from

$$\frac{b}{a} = e^{2\pi f_g \sqrt{\varepsilon_r}} \tag{2.3}$$

where $a$ is the inner radius. Thus, for $f_g$ = 67/377 and $\varepsilon_r$ = 2.2, we have $b/a$ = 5.2, so a reasonable configuration is $b$ = 8.5 cm and $a$ = 1.64 cm. .

The final result here is that the feed point will likely be electrically large, depending upon which assumptions are used for the dielectric breakdown of oil. And even if it can be shown that the feed point for the H4 (HASP) pulser can remain electrically small, it seems unlikely that the next generation pulser will be able to support an electrically small feed point. Thus, it is expected that a lens will in some cases be required to redirect the rays, as developed in [3].

Another method for reducing the electrical size of the feed point geometry is to reduce the feed impedance. It was shown in [1] that lower feed impedances in a coax can sustain a given peak power level in a smaller coax. (Ideally $Z_c \approx 30\ \Omega / \sqrt{\varepsilon_r}$ .) But lower impedances in the conical feed introduce excessive feed blockage. One way to lower the feed impedance without incurring additional feed blockage is to use an offset feed, which places the ground plane closer to the conical feed arms. We consider this strategy next.

## III. Offset Design

One way to lower to feed impedance of a half IRA is to use an offset feed. A lower feed impedance can sustain a given level of peak power in a smaller geometry, so this reduces the tendency of the pulse to disperse near the feed point. Recall from [1] that it was determined that the optimal feed impedance for maintaining maximum power for a given radius and peak electric field is about 20 ohms. Although we will not be able to get the feed impedance down to 20 Ω, it is worthwhile to investigate whether it can be reduced by a meaningful amount.

Consider first the impedance of a cone above a ground plane, as shown in Figure 3.1. This structure forms a transmission line whose impedance is [4, Eqn. 7]

$$f_g = \frac{Z_c}{Z_o} = \frac{1}{2\pi} \operatorname{arccosh}\left(\frac{\sin(\beta)}{\sin(\alpha)}\right) \tag{3.1}$$

Recall that if there are two thin feed arms arranged at ±45° to the vertical, as shown in Figure 3.2, then the impedance is reduced by a factor of two. For convenience, we have plotted in Figure 3.3 some values of impedance for a single-armed offset cone with various combinations of $\alpha$ and $\beta$.

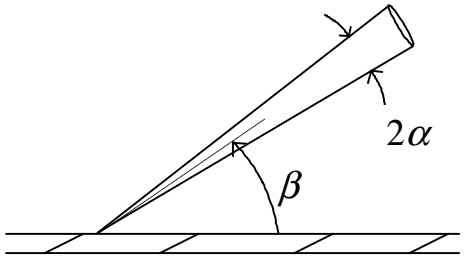


Figure 3.1. The angles associated with the feed geometry.

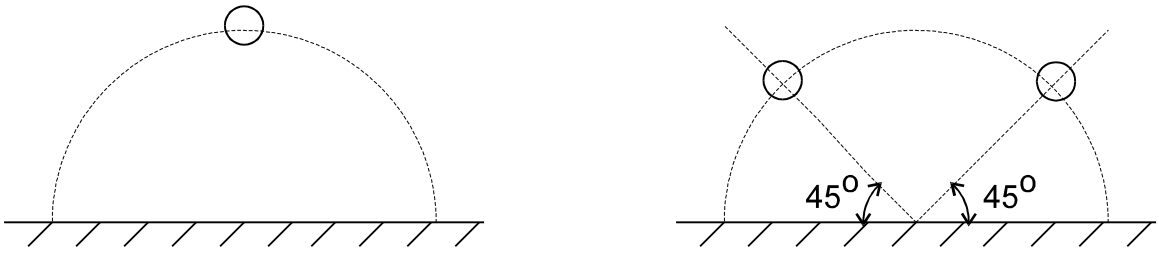


Figure 3.2. The structure on the right has one-half the impedance on the left, for small wire radii.

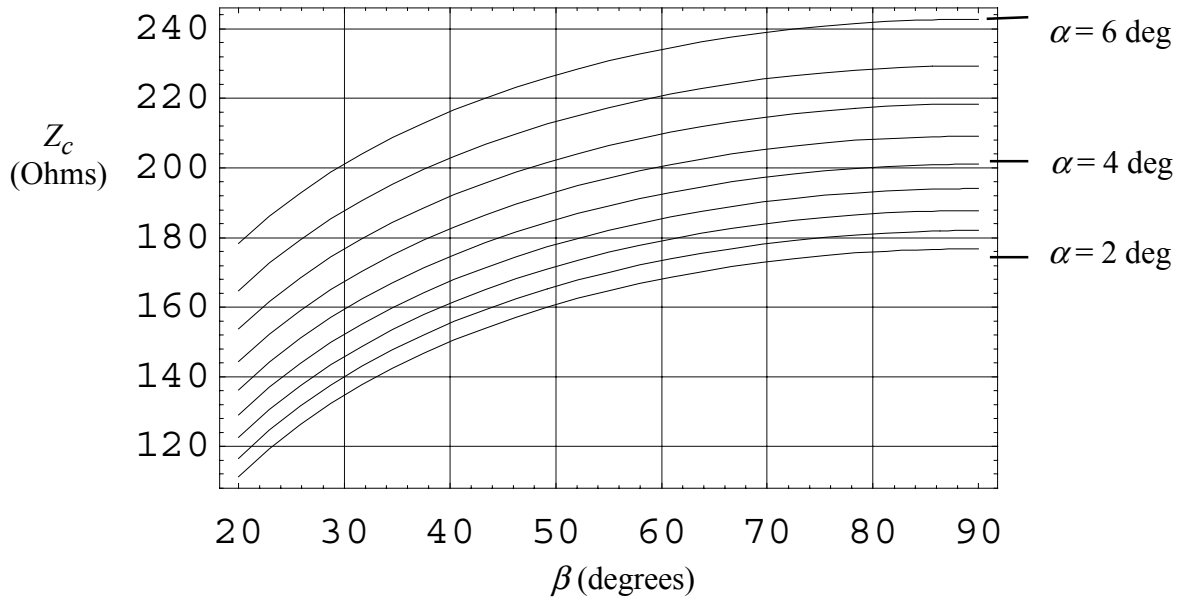


Figure 3.3. Offset cone impedance as a function of $\beta$, in half-degree increments of $\alpha$.

To see if this approach can be used to reduce the feed impedance a useful amount, it will be necessary to solve an example. A sample design using an offset feed is sketched in Figure 3.4. In this example, we have $\alpha = 4^o$ and $\beta = 36^o$, so $Z_c = 170\ \Omega$ for a single arm, or 85 Ω for two arms. Thus, we have reduced the original impedance in air from 100 Ω down to 85 Ω, or 85% of its original value. In oil, we have reduced the impedance from 67 Ω down to 57 Ω. Note that the high-frequency response of the offset design (Figure 3.4) is approximately the same as the high-frequency response for the simpler design (Figure 2.1). This is due to the fact that their effective heights are the same.

So what have we achieved by reducing the feed impedance from 67 Ω down to 57 Ω? To understand the effect, one must compare the efficiency factor of the two coax geometries. Recall from [1, Eqn. 4.6] that the efficiency factor was defined to be

$$\eta \;=\; \frac{Z_o^{1/2} P^{1/2}}{b\, E_{\max}} \;=\; \frac{2\pi f_g^{\,1/2} \sqrt{\varepsilon_r}}{e^{2\pi f_g \sqrt{\varepsilon_r}}} \tag{3.2}$$

After consulting [1, Figure 4.3] we find that the efficiency factor of an oil-filled coax at 67 Ω is 0.75, whereas at 57 Ω it is 0.89. This implies that one can reduce the outer radius of the feed coax, $b$, by a factor of 0.75/0.89 = 0.84, while maintaining the same peak power and peak electric field. This is arguably not a very large effect, when one considers the large extra volume required by the offset design. This suggests that an offset design may not be an effective use of the available space, and that if more space is available, it should be used to increase the reflector aperture size.

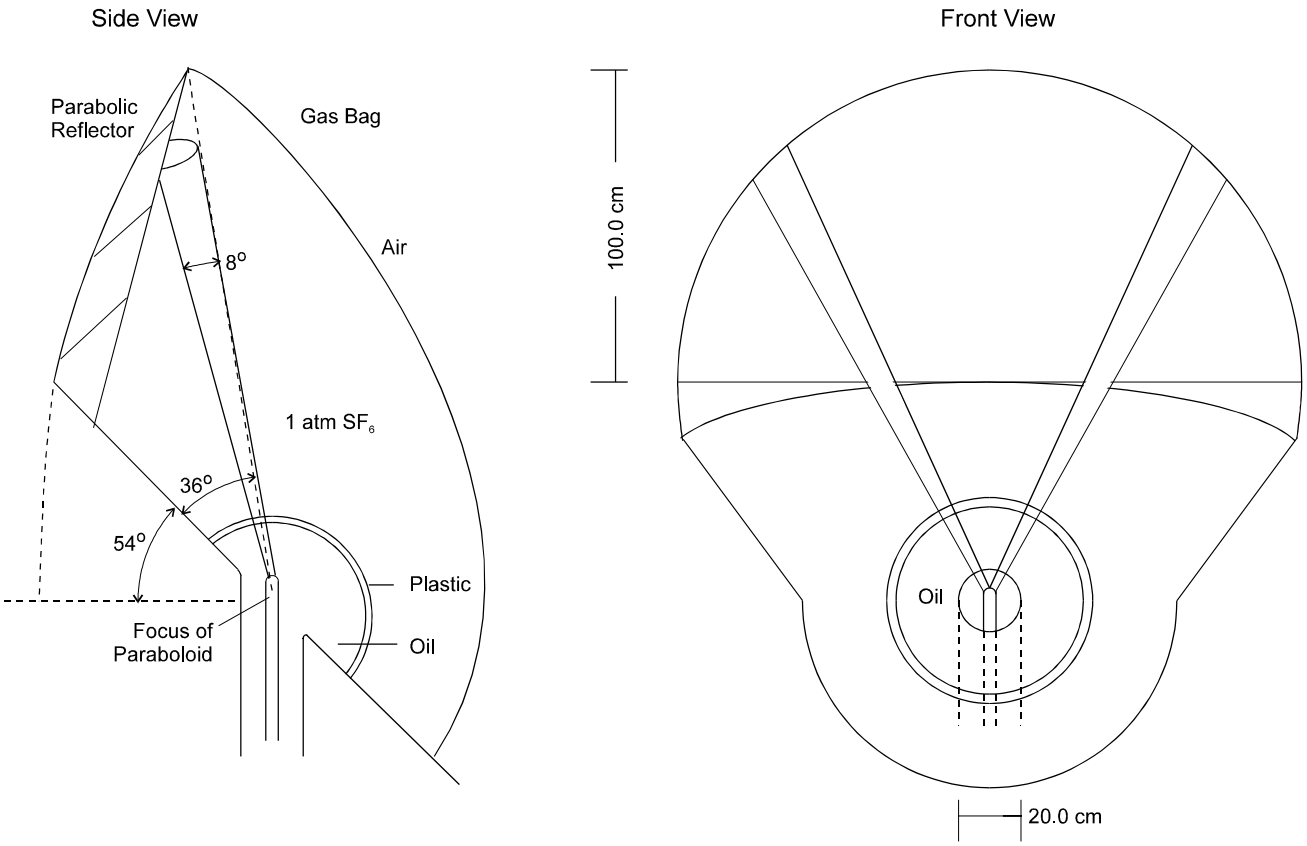


Figure 3.4. Offset Half IRA design.

### A. The Shape of the Offset Parabolic Reflector

There may still be reasons to use an offset design. An example might be if one wants to prevent an oil cap from blocking the aperture field. In this case, it will be useful to further specify the offset parabola surface. We assume here that we wish to radiate from an aperture that is a semicircle when viewed from the boresight radiation direction. A diagram of the intersection of the paraboloid and the semicircular cylinder is shown in Figure 3.5. Note that in Figure 3.4 the front edge of the paraboloid is drawn as a straight line, as viewed from the side. We prove now that this is indeed a line, and how to specify its location.

To show that the front slice of the paraboloid becomes a line when viewed from the side, we begin by expressing the equation of a paraboloid whose focus is at the origin. This is

$$z = -F + \frac{1}{4F}(x^2 + y^2) \tag{3.3}$$

where the geometry is as shown in Figure 3.5. We also have a right circular cylinder parallel to the $z$ axis with radius $R$ and offset from the origin by $y_o$. This is described by

$$x^2 + (y - y_o)^2 \;=\; R^2 \tag{3.4}$$

The intersection of these two equations when projected onto the *y*-*z* plane is found by eliminating *x* from the above two equations. After eliminating *x*, we find [5, p. 13]

$$y \;=\; \frac{2F}{y_o} z \;+\; \frac{4F^2 + {y_o}^2 - R^2}{2\,y_o} \tag{3.5}$$

This is a simple line in the *y*-*z* plane. This result is important because we can now describe how to cut a piece out of the paraboloid to build the surface. Two planar cuts are required, both of which project onto a line in the *y*-*z* plane (the side view). One cut is along the line described in (3.5), and one cut is through the intersection of the slanted ground plane and the paraboloid. This results in a surface whose forward edge sits flat on a table.

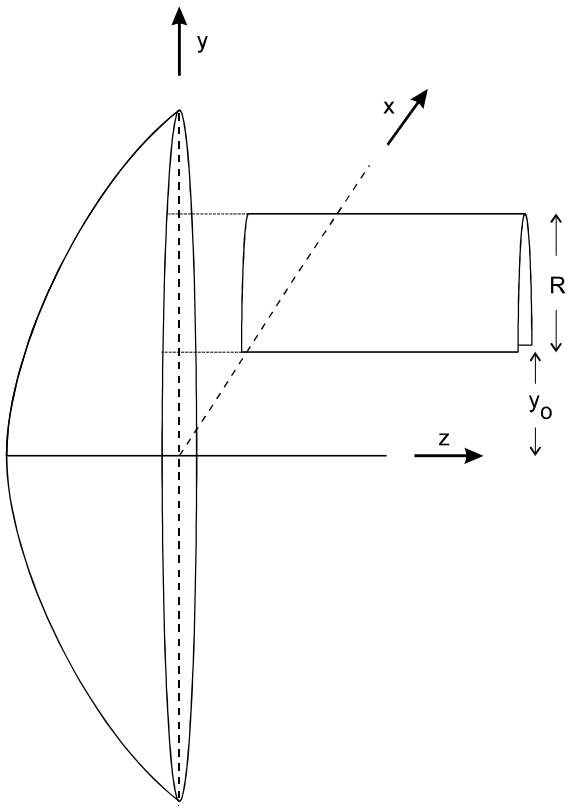


Figure 3.5. Intersection of a semicircular cylinder with a paraboloid.

## IV. Peak Electric Field at the "Hot Spot"

The location where dielectric breakdown is most likely to occur is where there is a final transition to air or $SF_6$, just after leaving the oil with a polyethylene container. A sketch of this location is shown in Figure 4.1. The size of the "oil bubble" that is required is determined by the peak electric field at this "hot spot." In general, it is preferable to keep the size of the oil bubble as small as possible, because it obstructs the radiated field after reflection by the paraboloid. To keep the size of this bubble small, we need to calculate the field generated at this hot spot.

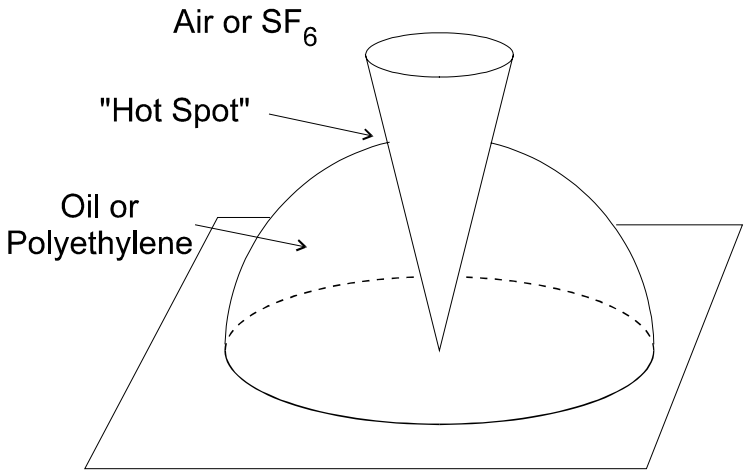


Figure 4.1. Location of the "hot spot."

In order to solve this problem, we first must identify the angles associated with the problem. The locations of the angles are shown in Figure 4.2. From [4], we find them to be

$$\begin{aligned} \beta &= 2\arctan\left[\frac{\tan(\beta_o/2)}{\tanh(\pi f_g)}\right] \\ \alpha &= \arcsin\left[\frac{\sin(\beta)}{\cosh(\pi f_g)}\right] \\ \beta_o &= \arctan\left[\frac{1}{2f_d - 1/(8f_d)}\right] \end{aligned} \tag{4.1}$$

where $f_g = Z_c/Z_o$, $Z_o = 376.727\ \Omega$, and $f_d$ is the $F/D$ ratio of the reflector. Note that $f_g$ refers in this case to a full version (both halves) of a two-armed IRA. Of the five variables that appear in the above equations, two are normally specified, and the remaining three are calculated from the equations. Note that $\beta$ is the is the angle to the center of the cone, and $\beta_o$ is the angle to the charge center of the cone.

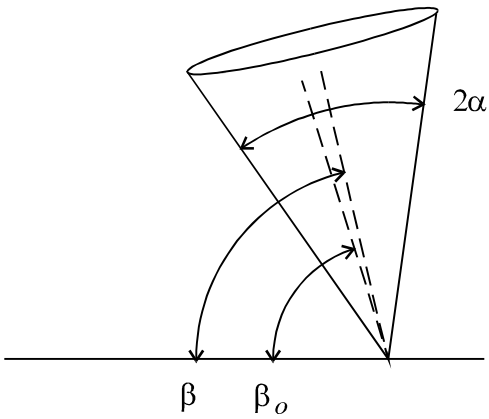


Figure 4.2. The angles associated with the feed arm. (The cone is drawn fatter than it should be for clarity.)

To find the field, we project the conical geometry onto an *x*-*y* plane in the normal manner as [6, 7]

$$\begin{aligned} x &= 2r_o \tan(\theta/2)\cos(\phi) \\ y &= 2r_o \tan(\theta/2)\sin(\phi) \end{aligned} \tag{4.2}$$

where $r_o$ is the radius where the dielectric terminates. The projection into a plane results in a circle over a ground plane, as shown in Figure 4.3. The parameters of the circle are [7]

$$\begin{aligned} b &= \frac{2r_o \sin(\beta)}{\cos(\alpha)+\cos(\beta)} \\ a &= \frac{2r_o \sin(\alpha)}{\cos(\alpha)+\cos(\beta)} \\ b_o &= \sqrt{b^2-a^2} = \frac{2r_o\sqrt{\sin^2(\beta)-\sin^2(\alpha)}}{\cos(\alpha)+\cos(\beta)} = \frac{2r_o\sqrt{\cos^2(\alpha)-\cos^2(\beta)}}{\cos(\alpha)+\cos(\beta)} \\ &= 2r_o\sqrt{\frac{\cos(\alpha)-\cos(\beta)}{\cos(\alpha)+\cos(\beta)}} = 2r_o\sqrt{\tan\left[\frac{\beta-\alpha}{2}\right]\tan\left[\frac{\beta+\alpha}{2}\right]} \end{aligned} \tag{4.3}$$

Once again, note that $b$ is the height to the center of the circle, and $b_o$ is the height to the charge center.

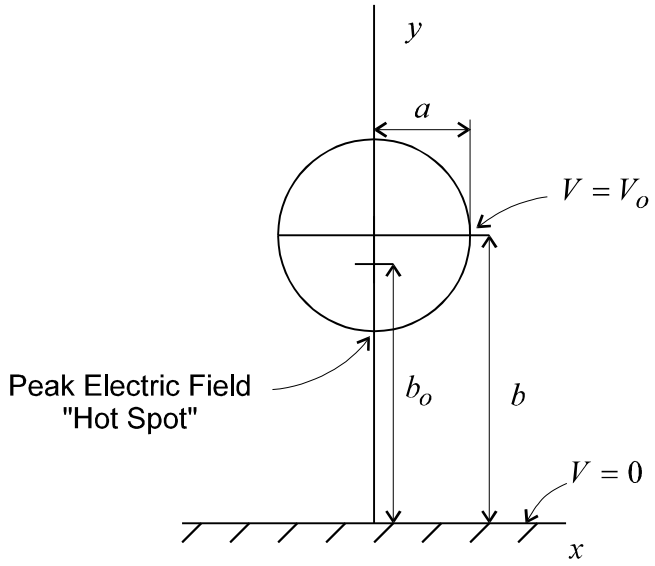


Figure 4.3. Projection of the spherical geometry onto a plane.

Let us now calculate the electric field at the "hot spot." First, we calculate the field in the projected plane at ($x$=0, $y$). This is obtained from [8] as

$$E_y(x=0,y) \;=\; -\frac{V_o}{\Delta u}\frac{\partial u(x=0,y)}{\partial y} \tag{4.4}$$

where

$$\begin{aligned} u(x=0,\,y) &= \ln\left[\frac{1+(y/b_o)}{1-(y/b_o)}\right] \\ \frac{\partial u(x=0,\,y)}{\partial y} &= \frac{(2/b_o)}{1-(y/b_o)^2} \end{aligned} \tag{4.5}$$

At the hot spot ($x$=0, $y$=$b$–$a$), so the derivative evaluates to

$$\left.\frac{\partial u}{\partial y}\right|_{(x,y)=(0,b-a)} \;=\; \frac{(2/b_o)}{1-((b-a)/b_o)^2} \tag{4.6}$$

It will be convenient later to express this in terms of angles. Using (4.3), we find

$$\frac{b-a}{b_o} = \frac{\sin(\beta)-\sin(\alpha)}{\sqrt{\sin^2(\beta)-\sin^2(\alpha)}} = \sqrt{\frac{\sin(\beta)-\sin(\alpha)}{\sin(\beta)+\sin(\alpha)}} = \sqrt{\frac{\tan\left[\frac{\beta-\alpha}{2}\right]}{\tan\left[\frac{\beta+\alpha}{2}\right]}} \tag{4.7}$$

It is also convenient to make a substitution for the tangent half angles as

$$q_1 = \tan\left[\frac{\beta-\alpha}{2}\right] \quad , \qquad q_2 = \tan\left[\frac{\beta+\alpha}{2}\right] \tag{4.8}$$

so we have

$$\begin{aligned} \frac{b-a}{b_o} &= \sqrt{\frac{q_1}{q_2}} \\ b_o &= 2r_o\sqrt{q_1 q_2} \end{aligned} \tag{4.9}$$

Substituting the above expressions into (4.6), the derivative simplifies to

$$\left.\frac{\partial u}{\partial y}\right|_{(x,y)=(0,b-a)} = \frac{1}{r_o\sqrt{q_1 q_2}\,[1-(q_1/q_2)]} \tag{4.10}$$

Finally, we calculate $\Delta u$ by evaluating $u(x, y)$ at $(0, b–a)$ and $(0,0)$ in equation (4.5). Using equation (4.9), we find

$$\begin{aligned} \Delta u &= u(x=0, y=b-a) - u(x=0, y=0) \\ &= \ln\left[\frac{1+\sqrt{q_1/q_2}}{1-\sqrt{q_1/q_2}}\right] \end{aligned} \tag{4.11}$$

If we now substitute (4.10) into (4.4), we find the peak electric field at the hot spot in the cylindrical geometry to be

$$E_y(x=0, y=b-a) = -\frac{V_o}{\Delta u}\frac{1}{r_o\sqrt{q_1 q_2}\;\;[1-(q_1/q_2)]} \tag{4.12}$$

where $\Delta u$ is as defined in (4.11). This is the peak electric field in the cylindrical geometry.

Next, we convert the field back into the spherical geometry. In this case, the peak electric field occurs at $(\theta,\phi) = (\beta\text{-}\alpha, \pi/2)$. The expression for the field there is

$$E_\theta(\theta, \phi=\pi/2) = -\frac{V_o}{r_o}\frac{1}{\Delta u}\frac{\partial u}{\partial \theta} = -\frac{V_o}{r_o}\frac{1}{\Delta u}\frac{\partial u}{\partial y}\frac{dy}{d\theta} = \frac{E_y(x=0, y)}{r_o}\frac{dy}{d\theta} \tag{4.13}$$

Thus, the conversion to spherical coordinates involves multiplying $E_y$ by a simple term. Using (4.2) we have

$$\begin{aligned} \frac{1}{r_o}\frac{dy}{d\theta}\bigg|_{\phi=\pi/2} &= \frac{1}{\cos^2(\theta/2)} \\ \frac{1}{r_o}\frac{dy}{d\theta}\bigg|_{(\theta,\phi)=(\beta-a,\pi/2)} &= \frac{1}{\cos^2[(\beta-\alpha)/2]} \end{aligned} \tag{4.14}$$

We now substitute (4.13) and (4.14) into (4.12), giving the peak field in the conical geometry as

$$\begin{aligned} E_\theta(\theta=\beta-\alpha,\phi=\pi/2) &= -\frac{V_o}{r_o} f_E \\ f_E &= \frac{1}{\Delta u\sqrt{q_1 q_2}\ \left[1-(q_1/q_2)\right]}\ \frac{1}{\cos^2[(\beta-\alpha)/2]} \end{aligned} \tag{4.15}$$

where the $q$'s are defined in (4.8) and $\Delta u$ is defined in (4.11). Note that the factor $\left[1-(q_1/q_2)\right]$ in the denominator is typically quite small, so this is the factor one must control in order to keep the peak field down. This is accomplished primarily by using larger $\alpha$'s, which implies lower impedances.

Let us now consider an example. We want the output cone to be rotationally symmetric, so this implies $\beta$ = 90°. We furthermore want to have a single-arm IRA whose full-IRA impedance is 400 Ω. This is the standard impedance that is used with IRAs most often. This corresponds to a Half-IRA whose input impedance is 200 Ω with a single arm, or 100 Ω with two arms. Note that we are specifying all our impedances for air or $SF_6$, since it is there that we are most concerned about breakdown. Note also that for the moment we consider just a single arm, keeping in mind that we can use symmetry at the end to add a second arm. Thus, we begin by specifying $\beta$ = 90° and $f_g$ = 400/376.727 = 1.0618.

Using (4.1), it is simple to find $\beta_o$ and $\alpha$ as 89.85° and 4.08°, respectively. To find $f_d$, one has to solve the final equation in (4.1) numerically. For this we find $f_d$ = 0.2506. It is interesting to note that *F/D* is close to, but not exactly 0.25. The confusion comes about because of a tendency to interchange $\beta$ and $\beta_o$, since they are so close.

Substituting these numbers into (4.15), we find for this case

$$E_\theta(\beta-\alpha,\pi/2) = -\frac{V_o}{r_o} f_E \quad , \qquad f_E = 4.22 \tag{4.16}$$

Let us now suppose that we wish to maintain a total of 100 GW on this single-armed structure. The voltage required is

$$V_o \;=\; \sqrt{PZ_c} \;=\; \sqrt{10^{11}\,\mathrm{W}\times 200\,\Omega} \;=\; 4.47\ \mathrm{MV} \tag{4.17}$$

Let us assume further that at the exit to the bubble we can sustain 500 kV/cm in 1 atm $SF_6$, or 50 MV/m. The radius required to hold this off is

$$r_o \;=\; -\frac{V_o}{E_{\max}} f_E \;=\; \frac{4.47\ \mathrm{MV}}{50\ \mathrm{MV/m}}\,4.22 \;=\; 0.38\ \mathrm{m} \tag{4.18}$$

Because of the aperture blockage associated with an oil cap of this size, we would like to explore alternative configurations.

As a second configuration, we can reduce the bubble size by using two arms instead of one (see Figure 2.1). We do this while keeping the same angular width feed arms, and while maintaining the 100 GW power level. This reduces the voltage on each arm by a factor of $1/\sqrt{2}$, so the outer radius is reduce by a similar factor, to a value of 0.267 m.

Although the second configuration reduces the bubble size, one can probably argue that it is still too large for a reflector with a 1-meter radius. This motivated us to consider designs in [3] that avoided the oil cap entirely. While a design without an oil cap has a reduced resistance to dielectric breakdown, one can argue that for pulses as short as 300 ps FWHM there is insufficient time for a pulse to cross the gap before the stress is reduced, so breakdown is unlikely anyway. Clearly, a final resolution to this question will require additional experiments on high-voltage dielectric breakdown with very short pulses.

## V. Radiated Field On-Boresight

Let us consider the fields that will be radiated by the half reflector IRA. We assume a two-arm configuration, each arm having an angular width of ±4º, so the input impedance is 100 Ω. These feed arms have same angular width as those used in a full two-arm IRA with an impedance of 400 Ω across the arms. The reflector has an $F/D$ of 0.25, with a radius of 1 meter. The antenna is driven with an integrated-Gaussian step function, with $t_d$ = 150 ps and peak voltage $V_o$ launched onto the TEM feed in air.

The theory for calculating the radiated field on boresight is only a small perturbation on the field calculated for the case with a full reflector [9]. Thus, we have a radiated field of

$$E(r,t) = \frac{a\sqrt{2}}{2\pi c\, f_g\, r}\left[\frac{dV(t-2F/c)}{dt} - \frac{c}{2F}\left[V(t)-V(t-2F/c)\right]\right] \tag{5.1}$$

where $V(t)$ is the voltage from the feed arms to the ground plane in air, and $f_g$ is 400 Ω / 376.727 Ω. Furthermore, $c$ is the speed of light in free space, $a$ is the reflector radius, and $F$ is the focal length. The driving voltage is assumed to be an integrated Gaussian of the form

$$\frac{dV(t)}{dt} = \frac{V_o}{t_d}\, e^{-\pi(t/t_d)^2}, \qquad t_{FWHM} = 0.940\, t_d \tag{5.2}$$

$$V(t) = \int_{-\infty}^{t} \frac{dV(t')}{dt'}\, dt', \qquad t_{10-90} = 1.023\, t_d \tag{5.3}$$

where $t_{FWHM}$ is the Full Width Half Max of $dv/dt$, and $t_{10\text{-}90}$ is the 10-90% risetime of $V(t)$. Note that with this formulation the peak voltage is $V_o$.

As an example, we assume the parameters of the H4 source discussed earlier. Thus, we assume 100 GW is launched onto the antenna, so $V_o$ = 3.2 MV. Furthermore, $a$ = 1 m, $f_g$ = 1.06, and $t_d$ = 150 ps. The resulting radiated field is shown in Figure 5.1, where we see the peak value of $rE/V_o$ is 4.6.

We can now define a figure of merit for the combination of source and antenna to be $r\times E$ in the far field on boresight. Using this definition, our $r\times E$ figure of merit is 14.7 MV. Of course, we have not yet included reflection losses from the lens, so our estimate is high, by perhaps ten percent. But this result is still noteworthy, when compared to the 4-meter diameter, 120 kV system built by D. Giri et al [10]. In that effort, they measured a peak electric field of 4.2 kV/m at a distance of 304 meters, so $r\times E$ = 1.26 MV. Thus, the figure of merit in our example is about ten times that of the earlier effort. Note, however, that the biggest reason for the improvement is that a much larger source is used in our example than in the earlier effort.

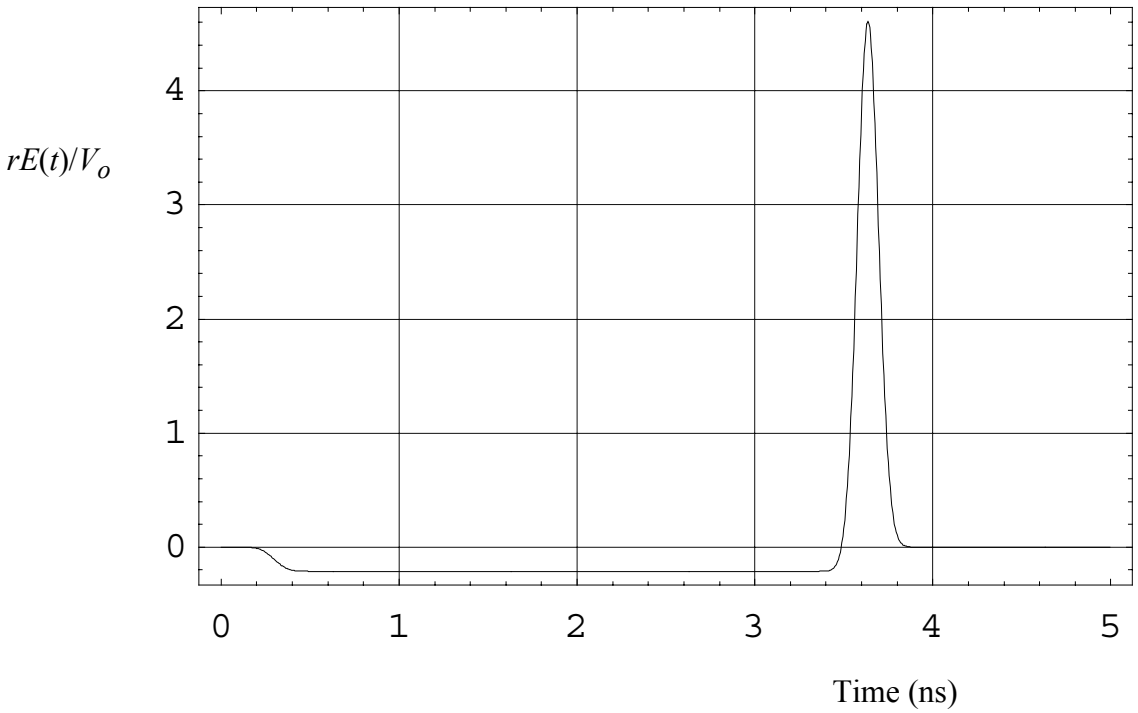


Figure 5.1. Radiated field on boresight for a 2 m diameter half IRA driven by a 150 ps risetime source. The peak is 4.6, with a $t_{FWHM}$ of 139 ps.

## VI. Radiated Field Pattern

We consider now how to calculate the fast part of the radiated waveform as a function of angle. The theory was developed in considerable detail in [11] for a full IRA with two round conical feed arms. We consider here the modifications required to have two feed arms with a half IRA. We begin by describing the solution for a full IRA with four arms, and then make modifications for the half IRA case.

When the conical geometry is projected onto a plane, we have an aperture field that is created from four conductors, as shown in Figure 6.1. The potential function is calculated by adding the potential for two two-wire problems that have been scaled and translated to their correct position. The potential function for a single two-wire problem, where the charge centers are located at ($x$=0, $y/a$ = 1), is

$$w_2(\zeta) \;=\; 2\,j\,\mathrm{arccot}(\zeta / a) \;=\; \ln\!\left(\frac{\zeta / a \;- j}{\zeta / a \;+ j}\right) \tag{6.1}$$

Here, $\zeta = x + j\,y$ is the location in the Cartesian coordinate space. This potential function was plotted in [11, Figure 2], so there is no need to repeat it here. The complex potential for the four-wire case is just a sum of two two-wire potentials that have been shifted and resized, i.e.,

$$w_4(\zeta) \;=\; w_2\!\left((\zeta / a + \sqrt{2}) / \sqrt{2}\right) \;+\; w_2\!\left((\zeta / a - \sqrt{2}) / \sqrt{2}\right) \tag{6.2}$$

This function is complex, i.e., has both real and imaginary parts. Let us therefore set

$$u(\zeta) \;=\; \mathrm{Re}(w_4(\zeta)) \quad , \qquad v(\zeta) \;=\; \mathrm{Im}(w_4(\zeta)) \tag{6.3}$$

We can plot contours of constant $u$ and $v$, and these are shown in Figure 6.2 for the upper right quadrant. The conductors correspond to a contour of constant $u$.

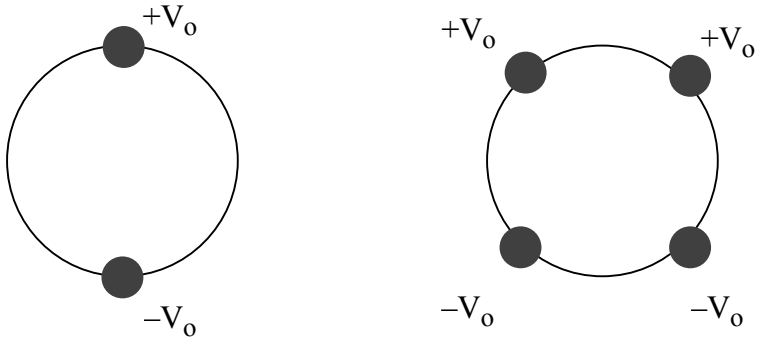


Figure 6.1. The apertures for a two-wire and four-wire configuration.

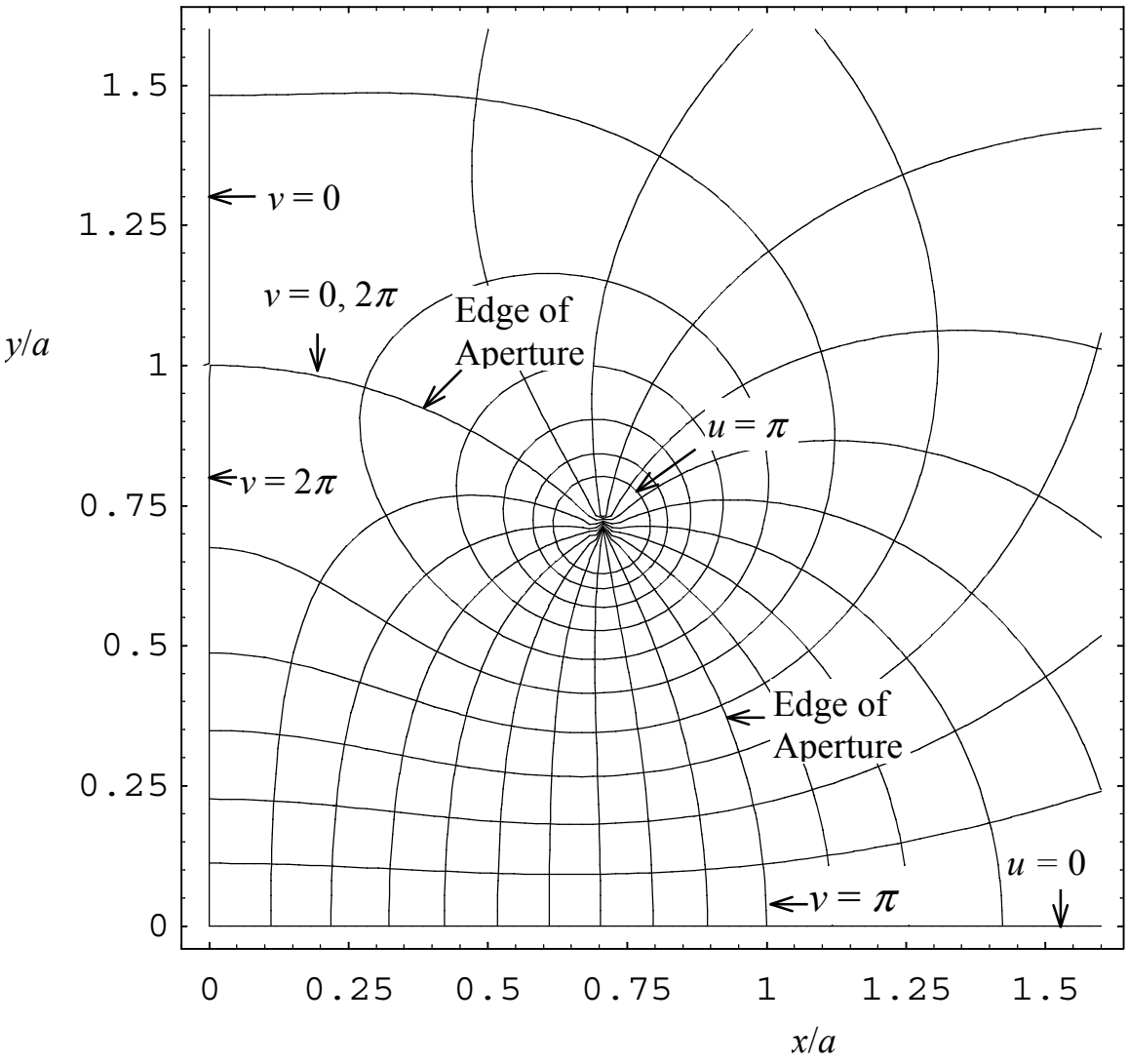


Figure 6.2. Contour map for $w_4(\zeta)$. Increments for $u$ and $v$ are $\pi/10$.

To calculate the radiated field, we need the aperture fields and the normalized aperture potentials. First, we find the aperture field is

$$E_y(x,y) = \frac{-(2V_o)}{\Delta u}\frac{\partial u(x,y)}{\partial y} \tag{6.4}$$

where $2V_o$ is the voltage between the top and bottom conductors, and $\Delta u$ is the change in $u$ between the two conductors.

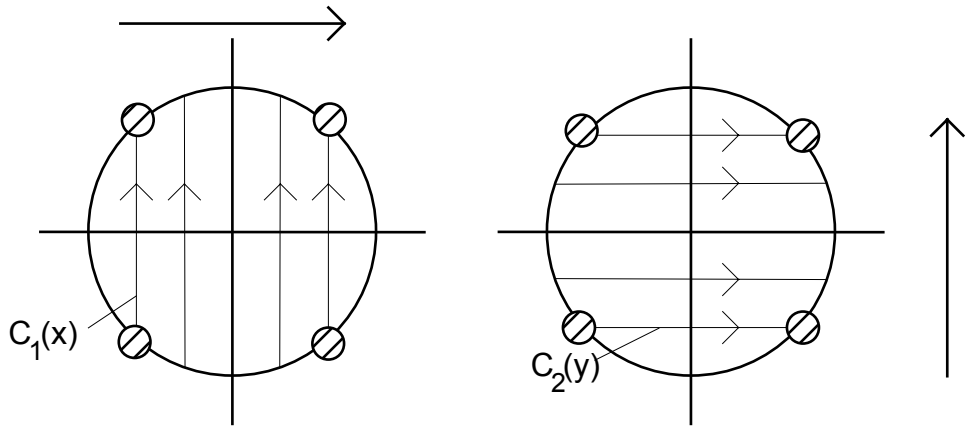


Figure 6.3. Locations of $C_1(x)$ and $C_2(y)$.

Next, we find the normalized potentials, which are integrals of electric field over linear paths in the aperture plane. The normalized potential for the H-plane calculation is

$$\Phi^{(h)}(x) \;=\; -\frac{1}{(2V_o)}\int_{C_1(x)} E_y\, dy \tag{6.5}$$

where the contour $C_1(x)$ is a vertical line cut through the aperture plane, as shown in Figure 6.3. To simplify this, one substitutes (6.4) into (6.5), generating

$$\Phi^{(h)}(x) \;=\; \frac{1}{\Delta u}\int_{C_1(x)} \frac{\partial u}{\partial y}\, dy \;=\; \frac{2}{\Delta u}\; u\left(x, \sqrt{a^2 - x^2}\right) \tag{6.6}$$

We can now calculate $u(x,y)$ as the real part of the potential function given in (6.2). Note that the value of $u(x,y)$ is a maximum when it cuts through the conductors. At this point, the value of $u(x,y)$ is $u_o = \pi f_g$. where $f_g$ is the relative impedance for a single pair of arms located on opposite sides of the circle (typically 400 Ω€/ 377 Ω). Note also that for values of $x$ that cut through the conductors, the normalized potential is unity. This normalized potential function is plotted in Figure 6.4, for a few different values of $f_g$.

The normalized potential for the E-plane is expressed as

$$\Phi^{(e)}(y) \;=\; -\frac{1}{(2V_o)}\int_{C_2(y)} E_y\, dx \;=\; \frac{1}{\Delta u}\int_{C_2(y)} \frac{\partial u}{\partial y}\, dx \tag{6.7}$$

where $C_2(y)$ is a horizontal linear cut through the aperture plane, as shown in Figure 6.5. To evaluate this, we require the Cauchy-Riemann relation for analytic functions,

$$\frac{\partial u}{\partial y} \;=\; -\frac{\partial v}{\partial x} \tag{6.8}$$

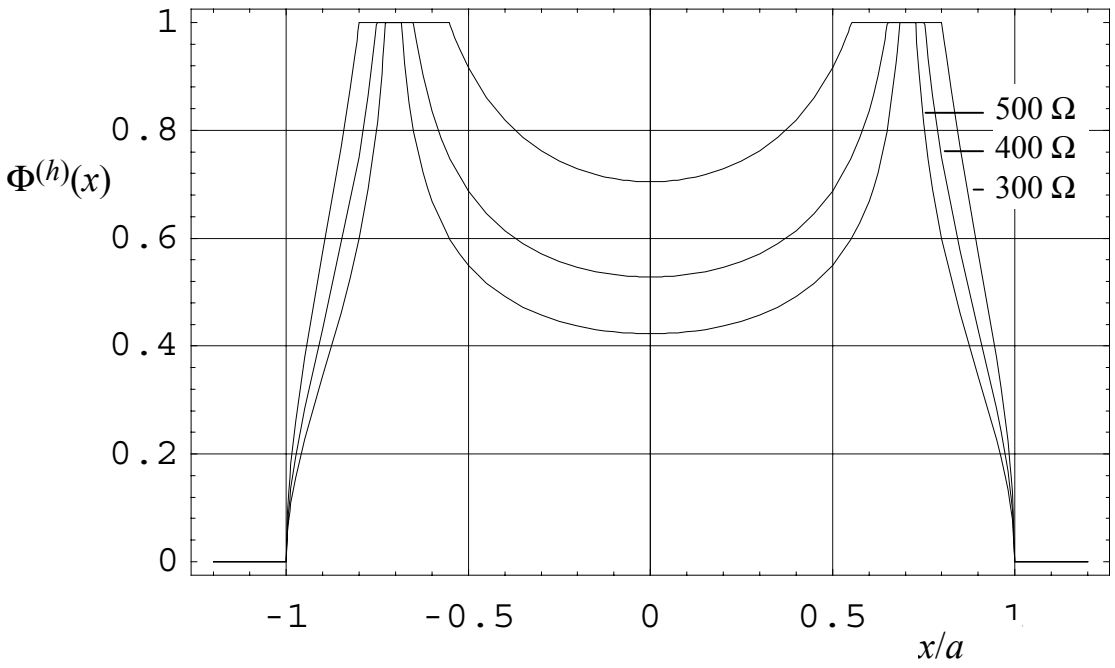


Figure 6.4. The normalized potential function of a full 4-wire aperture, $\Phi^{(h)}(x)$, plotted for a few different impedances.

We can now recast the integral as

$$\Phi^{(e)}(y) \;=\; \frac{-2}{\Delta u}\left[ v\left(\sqrt{a^2 - y^2}, y\right) \;-\; v(0, y)\right] \tag{6.9}$$

This is a particularly simple form, because the edges of the circular aperture are also lines of constant $v$. Thus, the normalized potential is evaluated analytically as

$$\Phi^{(e)}(y) \;=\; \begin{cases} 1/f_g & 0 \;\le\; |y|/a \;<\; 1/\sqrt{2} \\ 0 & \text{else} \end{cases} \tag{6.10}$$

We have plotted the normalized potentials for a few impedances in Figure 6.5. Note that our theory predicts an abrupt discontinuity in $\Phi^{(e)}(y)$ near the wires. In fact, there is actually a more smooth transition between the two values, but if the wire is thin, this is an excellent approximation.

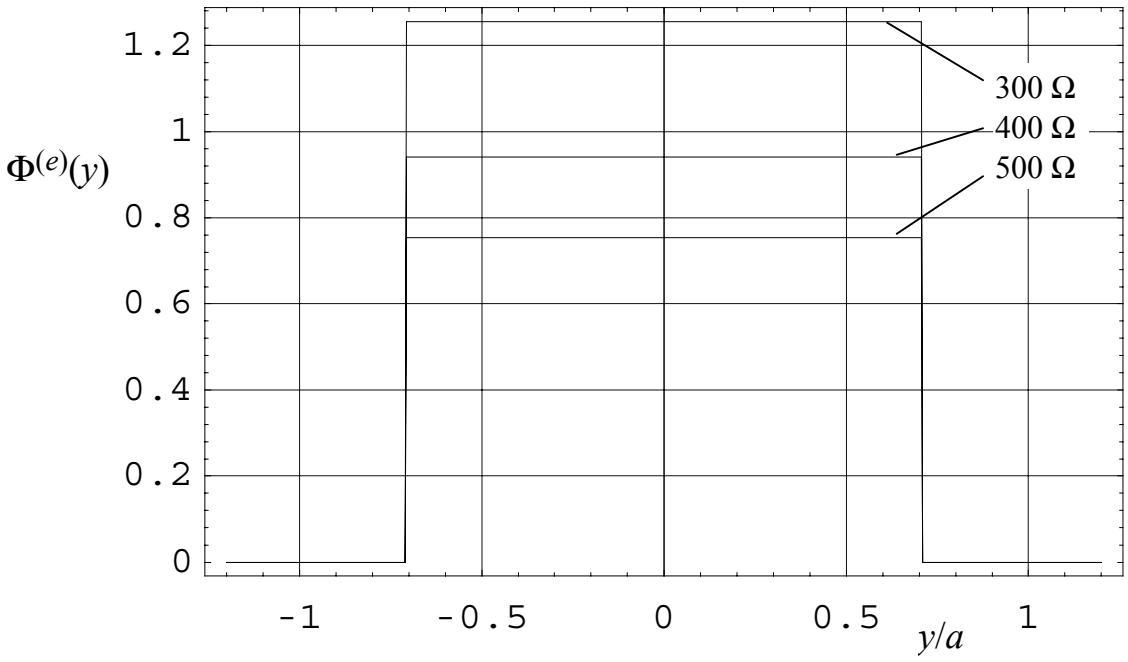


Figure 6.5. The normalized potential function of a full 4-wire aperture, $\Phi^{(e)}(y)$, plotted for a few different impedances.

With the normalized potentials calculated, we can now calculate the radiated field as a function of angle off boresight in the H and E-planes. The aperture field is created by a step voltage of magnitude $2V_o$ across the aperture, so from [11] we find

$$\begin{aligned} \vec{E}_{step}{}^{(h)}(r,\theta,t) &= \vec{1}_y \left(\frac{-(2V_o)}{r}\right) \frac{\cot(\theta)}{2\pi} \Phi^{(h)}\left(\frac{ct}{\sin(\theta)}\right) \\ \vec{E}_{step}{}^{(e)}(r,\theta,t) &= \pm \vec{1}_\theta \left(\frac{-(2V_o)}{r}\right) \frac{1}{2\pi\sin(\theta)} \Phi^{(e)}\left(\frac{ct}{\sin(\theta)}\right) \end{aligned} \tag{6.11}$$

This completes the calculation of the step response radiation for a full 4-wire aperture, before it is cut in half.

Next, we modify the above relationships to address the case of a half IRA, or half of a four-wire aperture. To do so, all that is necessary is to change the normalized potentials. The H-plane potential, $\Phi^{(h)}(x/a)$, is adjusted by dividing by 2, and the E-plane potential, $\Phi^{(e)}(y/a)$, is adjusted by constraining it to be nonzero only over the top portion of the aperture. Thus, we have

$$\begin{aligned} \Phi_{1/2}{}^{(h)}(x) &= \frac{1}{\Delta u}\; u\left(x, \sqrt{a^2 - x^2}\right) \\ \Phi_{1/2}{}^{(e)}(y) &= \begin{cases} 1/f_g & 0 \le y/a < 1/\sqrt{2} \\ 0 & \text{else} \end{cases} \end{aligned} \tag{6.12}$$

where the subscript "1/2" refers to a half aperture. These normalized potentials are plotted in Figure 6.6. They can now be used to calculate the step-response radiated field off-boresight as

$$\begin{aligned} \vec{E}^{\,(h)}_{step\,1/2}\;(r,\theta,t) &= \vec{1}_y \left(\frac{-(2V_o)}{r}\right) \frac{\cot(\theta)}{2\pi} \quad \Phi_{1/2}{}^{(h)}\left(\frac{ct}{\sin(\theta)}\right) \\ \vec{E}^{\,(e)}_{step\,1/2}\;(r,\theta,t) &= \pm \vec{1}_\theta \left(\frac{-(2V_o)}{r}\right) \frac{1}{2\pi\sin(\theta)} \quad \Phi_{1/2}{}^{(e)}\left(\frac{ct}{\sin(\theta)}\right) \end{aligned} \tag{6.13}$$

These are plotted in Figure 6.7. Note that $V_o$ is the potential between the ground plane and the feed arms, as one might expect.

To obtain the radiated fields, we convolve the step responses with the derivative of the driving voltage. To drive the antenna, we assume an integrated Gaussian with a peak magnitude of $V_o$ and a risetime of 150 ps. We have plotted the time response at $\theta = 0^o$, $2.5^o$, $5^o$, $10^o$ and $20^o$ away from boresight in the E and H planes, in Figure 6.8. Note that the H-plane response falls off more rapidly at wider angles, because the antenna aperture is more broad in the $y$ direction than in the $x$ direction. Note also that the peak field on boresight in Figure 6.8 is consistent with the peak field in Figure 5.1. This is noteworthy because the fields were calculated by using two very different techniques, and the results are still consistent.

## VII. Conclusions

We have considered a variety of design considerations relating to a half Impulse Reflecting Antenna. This included calculations of the dielectric strength of the feed, and a calculation of the peak field at the "hot spot," where a feed arm emerges from an oil cap. We also calculated the fields radiated both on-and off-boresight.


## Acknowledgments

We would like to thank Dr. Carl E. Baum, of Phillips Laboratory, for many helpful discussions relating to this work. We would also like to thank Mr. William D. Prather, also of Phillips Laboratory, for funding this work.

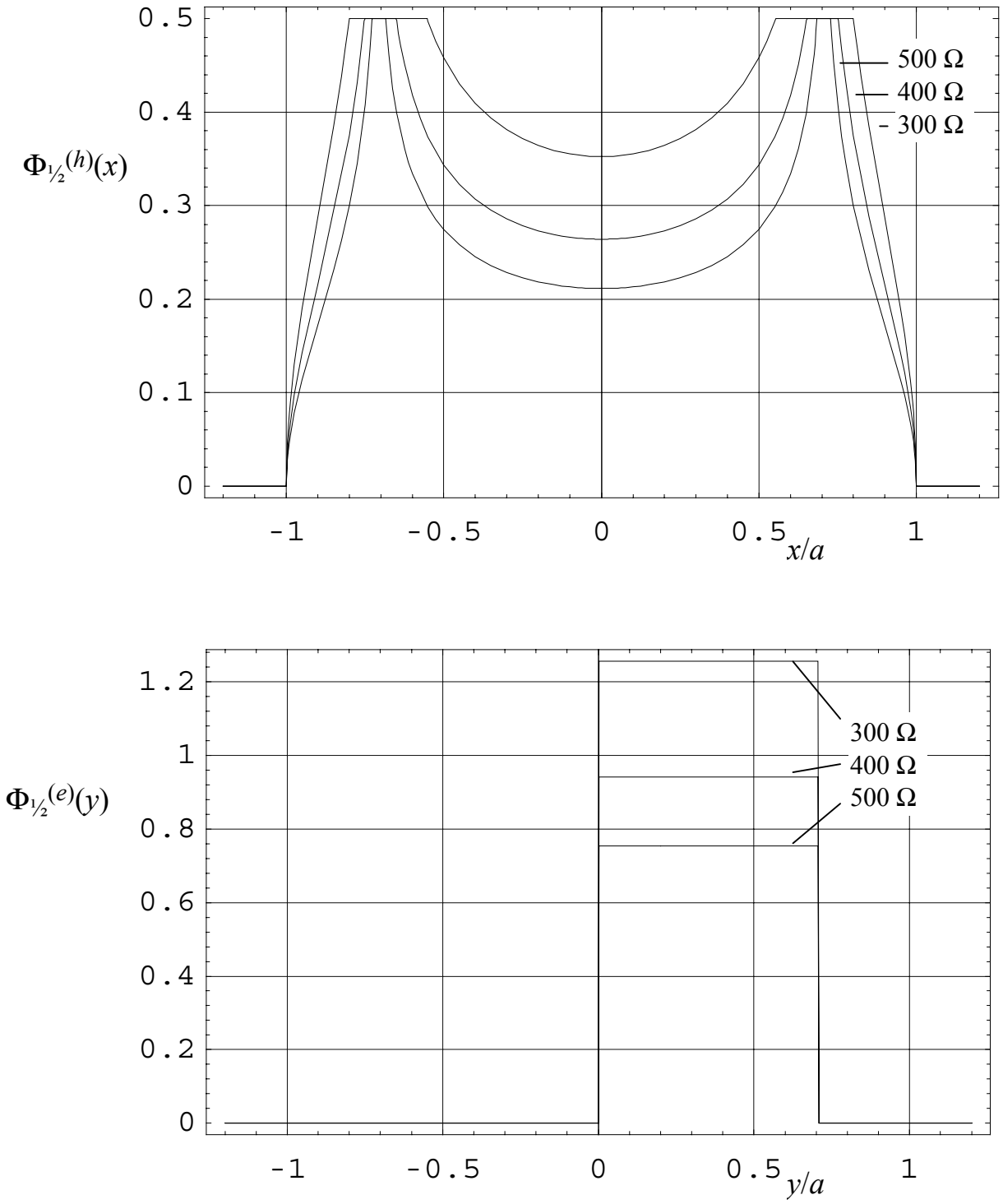


Figure 6.6. The normalized potential functions $\Phi_{1/2}^{(h)}(x)$ and $\Phi_{1/2}^{(e)}(y)$ for a few different impedances.

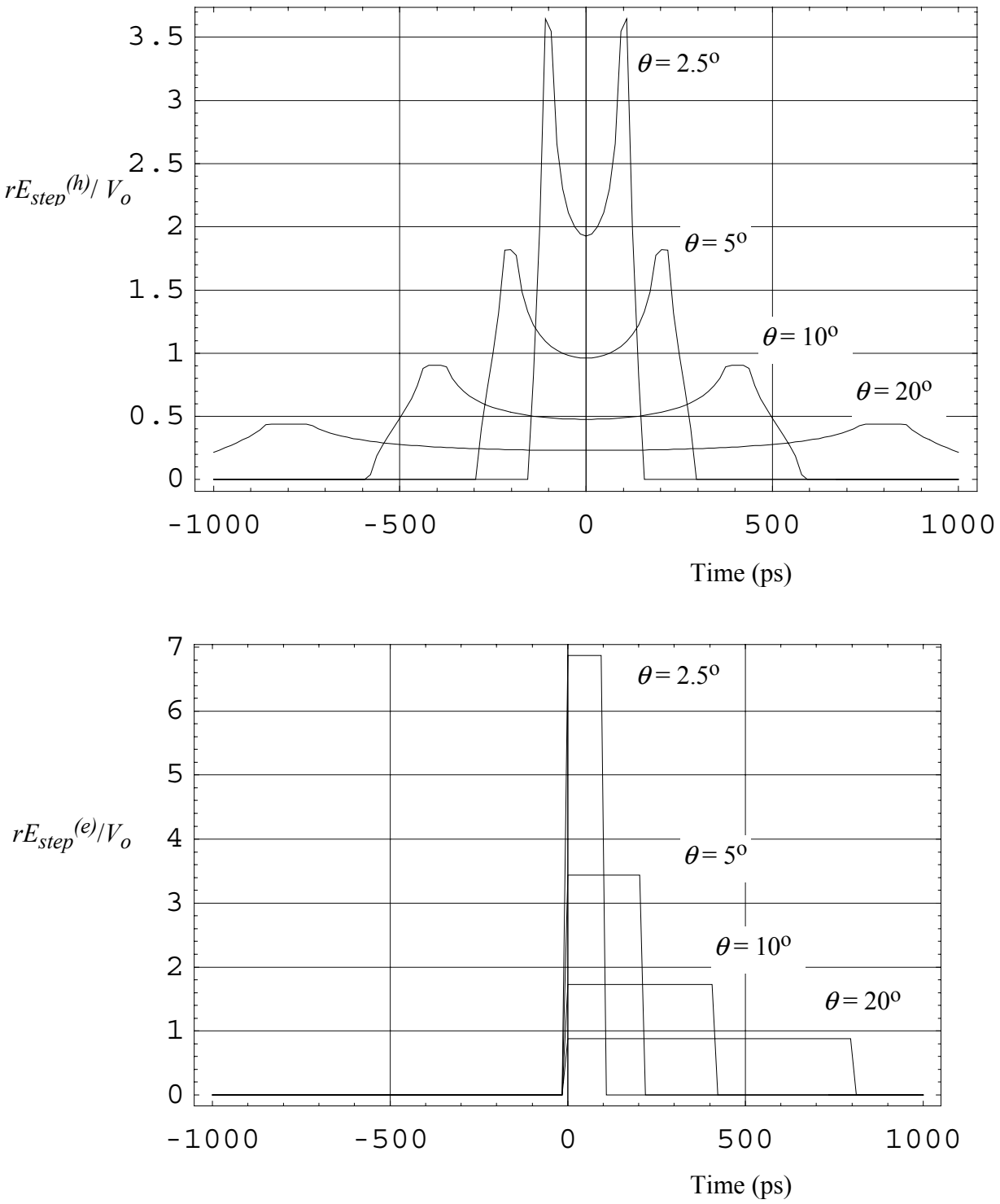


Figure 6.7. Step response of a half IRA in the H-plane (top) and the E-plane (bottom).

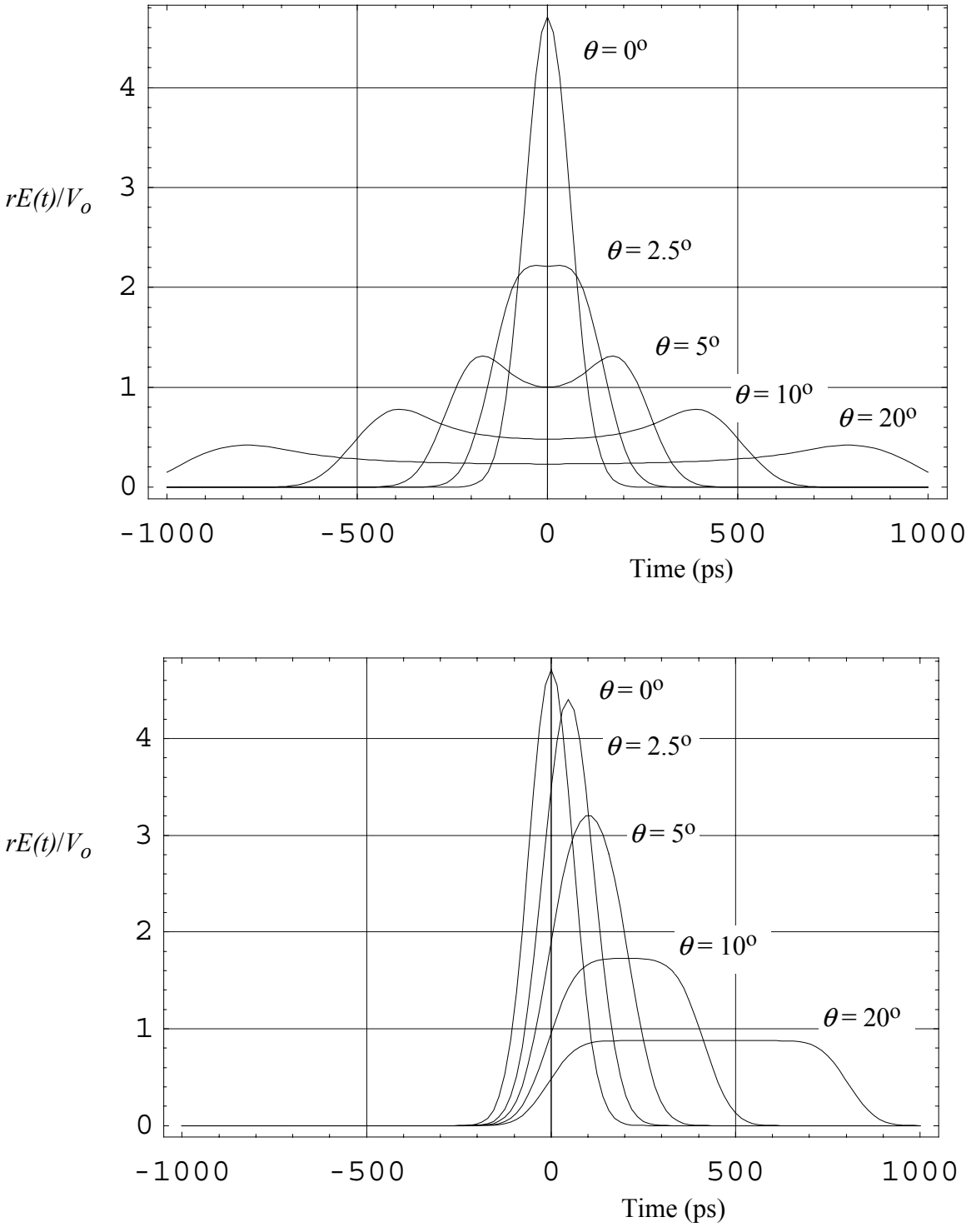


Figure 6.8. Fast part of the H-plane (top) and E-plane (bottom) radiated field for the half reflector IRA.

**References**


1. E. G. Farr, et al, Design Considerations for Ultra-Wideband, High-Voltage Baluns, Sensor and Simulation Note 371, October 1994.

2. C. E. Baum, Variations on the Impulse Radiating Antenna Theme, Sensor and Simulation Note 378, February 1995.

3. E G. Farr and C. E. Baum, Feed-Point Lenses for Half Reflector IRAs, Sensor and Simulation Note 385, November 1995.

4. E. G. Farr and C. E. Baum, Prepulse Associated with the TEM Feed of an Impulse Radiating Antenna, Sensor and Simulation Note 337, March 1992.

5. Y. Rahmat-Samii, "Reflector Antennas," Chapter 15 in Y. T. Lo and S. W. Lee, *Antenna Handbook*, Van Nostrand Reinhold, 1988.

6. W. R. Smythe, *Static and Dynamic Electricity*, Third Edition, 1989, p. 460.

7. R. W. Latham, M. I. Sancer, and A. D. Varvatsis, Matching a Particular Pulser to a Parallel-Plate Simulator, Circuit and Electromagnetic System Design Note 18, November 1974.

8. C. E. Baum, Impedances and Field Distributions for Symmetrical Two Wire and Four Wire Transmission Line Simulators, Sensor and Simulation Note 27, October 1966.

9. E. G. Farr and C. A. Frost, Compact Ultra-Short Pulse Fuzing Antenna Design and Measurements, Sensor and Simulation Note 380, June 1995.

10. D. V. Giri , et al, A Reflector Antenna for Radiating Impulse-Like Waveforms, Sensor and Simulation Note 382, July 1995.

11. E. G. Farr and C. E. Baum, The Radiation Pattern of Reflector Impulse Radiating Antennas: Early-Time Response, Sensor and Simulation Note 358, June 1993.